Photo-crosslinkable human amniotic membrane hydrogel for recovery from spinal cord injury

Tao Xu[1] , Chang-wei Yang[1] ,Yang Lu[1] , Heng Wang[1] , Cheng Chen[1] ,Yu-chen Zhou[1] ,Xiao-qing Chen [1] *

Abstract

The recovery and reconstruction of central nervous system function after spinal cord injury is a worldwide problem. The difficulty lies in the feasibility of new axons passing through the injured area and the negative effect of scarring after injury. As a biological material, the human amniotic membrane has the advantages of protecting nerve growth, inhibiting scar formation, and promoting neovascularization, but its weak physical properties have been difficult to apply in treating spinal cord injury. In this study, human amniotic membranes were first decellularized and chemically grafted with methacrylic anhydride. The composite was then photocrosslinked with gelatin methacrylate to prepare a cross-network biological complex. The complexes were used for in vitro and in vivo studies of spinal cord injury in rats. In the in vitro experiment, the composite scaffold inherited abundant biological factors from the amniotic membrane and had the physical properties of a hydrogel, which provided a good environment for the growth and development of neurons and blood vessels. In vivo, the composite reduced scar production and promoted the growth of new nerves. Composite scaffolds can stably simulate the extracellular microenvironment in spinal cord injury defects, regulate pathological changes and promote the generation of new

1:Affiliated Hospital of Nantong University, Medical School of Nantong University.
* Corresponding author at:
Department of Spine Surgery, Affiliated Hospital of Nantong University, Medical School of Nantong University, Nantong 226001, China.E-mail addresses：chenxiaoqing@ntu.edu.cn.

neurons. We conclude that decellularized human amniotic membrane hydrogels are promising biocomposite materials for central nerve repair after spinal cord injury.

Keywords: spinal cord injury · nerve regeneration · human acellular amniotic membrane · composite hydrogel· biological materials

Introduction

With the continuous development of tissue engineering and regenerative medicine in the field of nerve injury, an increasing number of biological functional materials have gradually entered the public vision in recent years. As the thickest basement membrane in the human body, the human amniotic membrane has been widely used in the fields of corneal transplantation, soft tissue injury healing, wound dressing preparation, cartilage repair and tendon repair in ophthalmology [1]. With further research, an increasing number of scholars have chosen to decellularize HAMs to improve their operability [2, 3]. Moreover, the immunogenicity of the decellularized human amniotic membrane was greatly reduced. Human acellular amniotic membrane (HAAM) has been used in cartilage regeneration engineering, vascular regeneration tissue engineering and other applications due to its excellent biological activity. In many studies, HAAM is usually applied directly to the wound and is sutured in place. Many studies have demonstrated that HAAM can promote wound healing, prevent infection, and reduce inflammation and scar formation [4]. However, as a film with poor mechanical properties, HAAM cannot be effectively used to treat defects caused by spinal cord injury, thus limiting the ability of HAAM to promote central nerve growth [5].

The extracellular matrix of HAMs did not change after acellular treatment of the amnion. The bioactive components that maintain HAAM mainly include collagen, fibronectin, laminin and hyaluronic acid. Among these collagens are types I, IV, V, and VI [6]. Hyaluronic acid (HA) is widely used in bioengineering to inhibit bacterial multiplication, promote mucosal recovery, and prevent scar growth. At present, many

studies have used HA as a substrate to load bioactive materials [7]. Fibronectin is widely involved in tissue repair and cell migration. A considerable number of studies have used it for the development of hemostatic materials. Collagen has hemostatic properties and is well tolerated and bioabsorbable. The cellular activities of epithelial cells depend on the action of collagen. Laminin is a bridge between the differentiation and adhesive activities of different cell types [8, 9]. Previous studies have shown that HAAM can promote angiogenesis and vascular remodeling by enriching angiogenic growth factors. Angiogenic growth factors, including basic fibroblast growth factor and vascular endothelial growth factor, are mainly derived from the basement membrane layer of HAAMs [10].

In response to the drawback of poor physical properties, many technical adjustments have been applied to HAAM [11]. First, HAAM was crushed, dissolved, and mixed with other biomaterials. In this process, the mechanical properties of HAAM were not significantly improved, and the extracellular machinery of HAAM was destroyed. Some researchers have mixed HAAM with other cells or biomaterials to form a new extracellular matrix for axon growth and regeneration [12]. However, in spinal cord injury, the injury site is relatively narrow, which easily leads to peripheral blood supply obstruction, tissue edema, and scar formation. Ordinary HAAM mixed materials cannot achieve stable degradation and full filling, so the therapeutic effect of various bioactive factors of the amniotic membrane is limited. In summary, how to improve the mechanical properties of HAAM while maintaining its biological activity has become the primary problem to be solved.

Chemical grafting of methacrylic anhydride (MA) to the extracellular matrix can fully retain its biological activity [13]. Moreover, the combination of biomaterials and hydrogels for enhancing mechanical strength is a promising approach for spinal cord injury (SCI) treatment [14]. Based on this concept, we selected gelatin methacrylate (GelMA) as the photocrosslinking carrier to ensure the release of its biological factors. At the same time, HAAM was chemically grafted with MA to form a two-component structure with GelMA instead of simple physical mixing (Fig. 1). The dialysis step in MA grafting can adequately eliminate the residual crosslinker. Rapid and stable

photocrosslinking can prevent instability of the mechanical properties of the composite and also avoid the damage of the biological activity caused by the long treatment process. Therefore, GelMA-HAAMMA has great potential as an ideal biocomposite scaffold for the treatment of spinal cord injury.

The microscopic morphology, mechanical properties, and degradability of GelMA-HAAMMA were evaluated in this paper. Furthermore, we verified the ability of GelMA-HAAMMA to coculture with neurons and to increase the proliferative activity of human umbilical vein endothelial cells (HUVECs) in vitro. In the in vivo study, a spinal cord defect model in Sprague–Dawley (SD) rats was selected to verify the ability of GelMA-HAAMMA to promote nerve regeneration after SCI by pathological sectioning, immunofluorescence staining and recovery of motor function at 4 weeks after surgery.

Materials and methods

Chemical reagents

Methacrylic anhydride (MA) was purchased from Shanghai Aladdin Biotechnology Company. Dulbecco's modified Eagle's medium (DMEM), neurobasal medium and fetal bovine serum (FBS) were purchased from Thermo Fisher Scientific Company. (China). Gelatin methacryloyl (GelMA) was purchased from Suzhou EFL Biotechnology Company.Dialysis replacement membranes were purchased from Jerope Bio-Tech, USA.Primary antibodies against GFAP and Tuj-1 were purchased from Wuhan Sanying Life Technology Company. (China). Secondary antibodies (goat anti-mouse IgGH&L (AlexaFluor®488), goat anti-rabbit IgGH&L (AlexaFluor®488), and goat anti-rabbit H&L (AlexaFluor®594)) were obtained from Shanghai Aladin Biochemical Technology Company. Trypsin-ethylenediamine tetraacetic acid (0.25%) and penicillin−streptomycin was purchased from Wuhan Prosser Life Technology Company. Optimal cutting temperature (OCT) compounds were obtained from Beijing Sola Biotechnology Company. A hematoxylin-eosin (H&E) staining kit was

purchased from Thermo Fisher Scientific Company. (China). A Masson's trichrome staining kit was purchased from Solaibao Technology Company. The cell scraper and neuron extraction kit were purchased from Suzhou Solaibao Biotechnology Company. Matrigel was purchased from Preferred Biotechnology (Nanjing, China).

Synthesis of GelMA-HAAMMA

Decellularization of the human amniotic membrane (HAM): The human amniotic membranes used in this study were donated by the research team of the Department of Obstetrics, Affiliated Hospital of Nantong University. Fresh human amniotic membranes were washed thoroughly with PBS solution containing 0.1% penicillin–streptomycin (v/v), cut into homogeneous sheets and stored at -80 °C for 2 hours. The mixture was then taken out and melted at 37°C. HAM was operated in three cycles of freezing and thawing.The samples were then mixed with 0.25% trypsin-EDTA solution for 12 h at 4 °C. Finally, the samples were washed with DMEM at 4 °C, and the epithelial cells were carefully scraped off with a cell scraper.The final product was weighed on a high-precision scale and dispensed in sterile Petri dishes containing ultrapure water. The weight of HAAM in each dish was approximately 1g.

Identification of HAAM: The research team randomly selected frozen sections from at least 3 different sets of samples for staining. Each slice contained at least 1 cm^2 of HAAM. Following the standard hematoxylin and eosin (H&E) protocol, the successful decellularization of HAAM sections was verified under the microscope (Leica dm3000, Clinical Trial Center, Affiliated Hospital of Nantong University) after dehydration with an alcohol gradient, washing with xylene, and sealing with neutral resin [10].

Synthesis of HAAMMA: Phosphate buffer solution (PBS) was used as a solvent to make the MA 4% (v/v) mixed solution, and then HAAM was completely immersed in the solution and thoroughly stirred in a ventilated environment at 4 °C. We stirred the

mixture every 2 hours at 4 °C. Chemically grafted HAAMMA was obtained after 8 hours. Subsequently, HAAMMA was washed repeatedly with PBS, loaded into dialysis bags (with a truncated molecular weight of 14-16 kDa) and dialyzed in ultrapure water for 36 hours to remove unreacted MA. The samples were lyophilized and stored [15-17].After weighing, each stored sample was 250mg.

Chemical grafting modification of HAAM: The samples of HAAMMA obtained in the previous step were dried in a drying box at 37 °C for approximately 30 minutes, after which the team members added potassium bromide powder (mass ratio 1:100) (BrK, Shanghai Aladdin Reagent Company.) and ground the mixture evenly[18]. The prepared product was put into a Fourier transform infrared spectrometer for analysis (FTIR, Tianjin Jingtuo Instrument Company., China). The resolution of the instrument was set to 4 cm^{-1}, and the scan range used for the measurements was 400 cm^{-1} to 4000 cm^{-1} (Number of scans: 32. Sampling gain: 1.0. Moving mirror speed: 0.4747. Detector: DTGS KBr. Aperture: 100.00).

Synthesis of GelMA-HAAMMA: Lyophilized gelatin methacrylate (GelMA, 500 mg) was soaked in 10% (w/v) PBS. GelMA in PBS was heated in a water bath at 70 °C for 30 minutes until completely dissolved. The solution was removed from the water bath and returned to room temperature. Lyophilized HAAMMA (250 mg) was added to the above solution. Right after that, lithium phenyl (2,4,6-trimethylbenzoyl) phosphinate (LAP, 0.1% (w/v)) was added. In a biosafety cabinet, the mixed samples were continuously irradiated with a UVLED point light source (395-480 nm, Suzhou Yongqin Equipment Company., China) for 60 seconds to form a 2-mm-thick gel. Finally, we dispensed the gel with a sterile instrument at room temperature. One part of the gel was used to tamponade the SCI model, and the other part was lyophilized at -80 °C for further verification [17].

Characterization and physical properties of GelMA-HAAMMA

SEM analysis: Our research team chose SEM to observe the characterization of the mixed material**.** The mixed material was first cut into 2 mm×2 mm films and fixed on the sample stage, and then the surface impurities were removed by washing with high-pressure nitrogen gas. The immobilization reagent was a conductive binder [19]. Our research team sprayed the surface of the sample samples with gold (20 mA, 90 s) with a spray plating machine and observed them under an S-5000 scanning electron microscope (Guoyi Electronics, China).

Identification of the mechanical properties: We set the experimental groups as HAAM, HAAMMA, GelMA, and GelMA-HAAMMA groups. At least three independent samples of 50 mm and 12 mm in length and width were selected for each set of materials. The test temperature was 25 °C with an ambient humidity of 35%. First, we set the clamping distance of the machine to 30mm. Next, the sample was fixed with a clamped metal frame and the head velocity was set to 10mm/min. The test was started with an initial tensile force of 6mN and a stepwise applied force gradient of 0.50mmN/min. The test was performed with a WSD series tensile testing machine (Wanchen Company., China) until the sample broke. Stress−strain curves were recorded for each sample, and their fracture strain values were calculated [17].

Degradation of GelMA-HAAMMA: Experimental grouping was consistent with that described above. We selected at least five random samples per group to determine the degradation rate of GelMA-HAAMMA. The weight of each group of materials was not less than 250mg. The mixed material was weighed to record the initial mass (W0), which was embedded subcutaneously in SD rats with SCI, and the residual mass (W1) was recorded at 0, 2, 4, 6, 8, 10, 14, 18, and 21 days. The material degradation rate was calculated as [(W0 - W1)/W0] × 100%[20, 21]. The

experimental environment was the standard animal feeding environment in the Animal Experimental Center of Nantong University. The experimental animals were all mature SD rats with moderate body weight. The rats used for measurements were randomly selected experimental SD rats without skin-related diseases.

The swelling rate of GelMA-HAAMMA: To measure the swelling rate, a total of 5 groups of GelMA-HAAMMA were prepared by our research team. The samples from each group were lyophilized, weighed (W2) and put into a certain amount of PBS solution. The samples were removed at 2, 4, 6, 12, 24, and 36 hours, and the surface was dried and weighed again (W3). Each group of materials was returned to PBS at the end of each weighing, and swelling was calculated as $[(W3 - W2)/W2] \times 100\%$ [22]. The final data were processed using Graph-Pad Prism 8.0 software (San Diego, United States).

In vitro studies

Coculture of GelMA-HAAMMA and neurons: To verify the support and trophic effects of the composite hydrogel scaffold on neurons, neurons were extracted from neonatal 0–3d Sprague–Dawley (SD) rats. The cell culture plates were coated with 20-fold diluted polylysine (10 mg/ml) for 3 hours in a cell incubator at RT. Finally, the liquid was aspirated, and the plates were washed three times with PBS. The cell slides were placed into each well plate for further planting. To verify the effect of coculture, we overlaid GelMA-HAAMMA composite hydrogels on a portion of the fixed cell slides. In another part of the well plates, only conditioned medium was added. Subsequently, the implant solution was supplemented with DMEM/F12 (42 ml), FBS (fetal bovine serum, 7 ml), 1% (v/v) penicillin–streptomycin, and L-glutamine (0.5 ml). Finally, the culture medium was supplemented with neurobasal medium (48 ml), B27 (1 ml), L-glutamine (0.5 ml), and 0.1% (v/v) penicillin–streptomycin. The left and right cerebral hemispheres of neonatal SD rats were exposed, the superficial brain

tissue was removed, and the crescent-shaped hippocampus was separated and placed in D-Hank's balanced salt solution. The blood vessels and meninges of the hippocampus were removed and placed into a centrifuge tube containing 4 ml of implant fluid.

The mixture was mechanically blown 20-40 times, followed by centrifugation for 5 min (1000 RPM). The supernatant was removed, 0.125% trypsin was added to the remaining liquid, the mixture was blown 20 times, and the mixture was placed in a cell incubator at 37 °C for 5 minutes. The mixture was taken out from the cell incubator and trypsin digestion was terminated by the addition of DMEM. The mixture was filtered through a 200-mesh sieve and seeded in Petri dishes at a cell density of $1x10^8$. The obtained cells were placed in culture medium and cultured for 4-5 hours, and the other cells that had adhered to the wall were discarded and centrifuged for 6 minutes (800 RPM). The supernatant was discarded, and subsequently, we seeded the remaining cells in pretreated cell well plates with culture medium. After the cells were fully adherent and grown, we first performed immunofluorescence staining of neuron-specific antibodies to verify the purification rate of neurons. According to the periodicity of neurons cultured in vitro, we chose to test the survival of neurons for three days to avoid the influence of culture medium toxicity on the experimental results [23]. At least 5 different cell slides from each of the 2 sets of well plates were selected for trypan blue staining on day 1 and day 3 of co-culture. Stained cells were observed and measured with a cell counter (Rayward company, Shenzhen, China).

Tube formation assay and cell migration assay: HUVECs were donated by the research team of the Department of Obstetrics and Gynecology, Affiliated Hospital of Nantong University. HUVECs were cultured in endothelial cell culture medium (5% fetal bovine serum and 1% penicillin−streptomycin) at 37 °C with 5% carbon dioxide.

For cell migration assays, HUVECs were seeded in 6-well plates (1.5×10^5 cells/well) and cultured until 100% confluence. The experimental groups were control

group, GelMA group and GelMA-HAAMMA group. Five parallel scratch-holes were then made in each well with a 100 μL pipette tip, and 1 mL of medium was added to each well, some of which contained a GelMA-HAAMMA composite scaffold (50mg) (n = 6). One of the remaining 6-well plates was supplemented with only 100 μL medium as a control, and the other was supplemented with GelMA (50mg) and 100 μL medium. Migration rates were observed under a light microscope after 24 h and measured immediately by using ImageJ software [10].

For angiogenesis experiments, we first added 50 μL of Matrigel to each well of a 96-well plate and waited for gel formation at 37° C. HUVECs were starved for 24 h and then added to 96-well plates (cell density $2x10^4$), 100 μL of medium was added to each well, and GelMA-HAAMMA was simultaneously added to each well of the plates (n = 3) [24]. The grouping of this experiment was consistent with cell migration assays. Angiogenesis was observed after 6 hours using an inverted light microscope (Olympus, Japan).

In vivo studies

The experimental animals in this study were all SD female rats (8 weeks old, weighing approximately 250 g). The animals were fed in an animal laboratory environment at 25 °C. The animal laboratory was equipped with a 12-hour light-dark cycle (8 a.m. to 8 p.m.). All the experimental procedures were performed in accordance with the Guide for the Care and Use of Laboratory Animals of the National Research Council. The animal ethics approval was approved by the Animal Care and Use Committee of Nantong University (Nantong, China) (220203322/22020214810).

In the simulation of spinal cord injury, our research team chosed a laminectomy of T10 segment. Before surgery, we anesthetized female SD rats via an intraperitoneal injection of 25 mg/kg anesthetics (sodium pentobarbital). The spinal cord was dissected evenly from the middle to the left side using a designed surgical scalpel,

separated by approximately 2 mm, resulting in defects in the left hemisphere of the rat spinal cord (Fig. 9A). SD rats were randomly divided into four groups with 15 rats in each group: a sham operation group with laminectomy only (sham group), a spinal cord injury group (SCI group), a GelMA group implanted with GelMA hydrogel, and a GelMA-HAAMMA group implanted with GelMA-HAAMMA composite hydrogel scaffold. The experimental SD rats were all carefully sutured to the muscle, fascia and epidermis, and the incisions were sterilized with iodine. To prevent infection and reduce pain, our research team injected rodents with buprenorphine and penicillin. After surgery, the rats were assisted in manually expelling urine from the bladder (three times/day) until urination returned to normal. At the 4-week postoperative time point, we euthanized the SD rats and obtained spinal cord tissue by dissection [25].

Postoperative functional recovery

In order to observe the functional recovery after spinal cord injury, the Basso, Beattie and Bresnahan (BBB) score was selected as the evaluation standard. BBB score is a rating scale ranging from 0 to 21. At 0, 1, 3, 7, 14, 21 and 28 days after SCI, the SD rats with SCI were allowed to roam freely in a closed environment for statistical observation. The personnel responsible for observing and scoring were unaware of the grouping of SD rats. Each group of SD rats was handled by three randomly assigned team members. The three members counted separately and did not communicate with each other about the results.

Histology of the spinal cord

At 4 weeks after SCI, we euthanized the SD rats and perfused the hearts with normal saline (200ml), followed by fixation with 4% paraformaldehyde. The members of the spinal cord containing the lesion site were removed by dissection, fixed with 4%

paraformaldehyde for 24 h, and then immersed in sucrose solution at different concentrations for dehydration. The spinal cord was encased in OCT. The tissues were processed in a cryomicrotome (lica-cm1950, Clinical Experimental Center, Affiliated Hospital of Nantong University) to obtain 8-12 μm thick coronal sections.

H&E and Masson staining

According to the standard protocol of Masson staining preparation and hematoxylin and eosin (H&E) staining, our research team randomly selected frozen sections from each experimental group for staining. After dehydration and fixation, the prepared sections were photographed with a light microscope (Leica dm3000) and analyzed with ImageJ software (National Institutes of Health).

Immunofluorescence staining of spinal cord sections.

We thawed the frozen sections for 35 min at RT and washed them with PBS. Next, the sections were incubated with 0.3% Triton X-100 containing 10% goat serum for 60 min at RT. Subsequently, we added the primary antibody to the slides and incubated them at 4° C for 16 h before adding the secondary antibody. After incubation for 2 h at RT, we washed the sections three times with PBS and stained the nuclei with DAPI. All the sections were observed under a Keyence fluorescence microscope and photographed.

Statistical analysis

Statistical analyses were conducted by using Graph-Pad Prism 8.0 software (San Diego, United States). For the sample-size calculation, the statistical power was set at 0.90, and the significance level was set at 0.05. We calculated the corresponding

minimum sample size based on the effect size of the different experiments. The data of each group were calculated as the mean ± standard deviation (SD). Statistical differences between groups were compared by using variance (ANOVA). Two-way repeated-measures ANOVA was used to analyze BBB scores. We used the SNK-q test to compare the means of multiple groups of data. $P<0.05$ was considered to indicate statistical significance, and at least three trials were performed for each experiment.

Results

Preparation of HAAM and HAAMMA

As shown in the upper part of Fig. 2A, freshly obtained HAM is a pink film, consistent with its nature as the thickest basement membrane in the human body. After the decellularization steps described above, as shown in the lower part of Fig. 2A, the successfully decellularized HAM became transparent and significantly reduced in weight and could float in the stored ultrapure water. Fig. 2B shows the H&E staining verification we performed to verify HAM decellularization. As shown above, nuclei labeled with hematoxylin can be seen in the stained image of normal HAM. Nuclei were neatly arranged in the epithelial layer of HAM. In the lower panel, however, the number of nuclei in the staining result is 0 (n = 5). Therefore, we determined from the double verification of gross observation and stained images that HAM had been successfully decellularized into HAAM. This confirmed the successful preparation of HAAM [10].

Fig. 2C shows the electron microscopy verification of HAM and chemically grafted HAM. The upper figure shows the cell-free structure and fibrous connections of HAAM. The lower part shows the structure and fibrous connections of HAAMMA. By comparison, it was found that the backbone structure and fiber connections in HAAMMA were not changed or even destroyed after chemical grafting. Fig. 2D shows the results of IR spectra to judge whether the grafting of MA is effective. The

upper figure shows the distribution of the characteristic peak of the IR spectra of HAAM. The amide A band of normal HAAM is concentrated at approximately 3290cm^{-1}. The peak value is mainly determined by the N-H vibration contraction. The lower figure shows that there was no significant destruction or change in the backbone structure of HAAMMA, whose characteristic peak of acrylamide appeared at 3396 cm^{-1} [15, 17]. This indicates that the grafting of MA was successful.

Representation of GelMA-HAAMMA

Due to the dense network structure of traditional biomaterial scaffolds, it is difficult for newborn cells to freely pass through them. Fig. 3A and B show the SEM results of HAAM and HAAMMA, respectively, both of which show a porous fiber network structure. This confirms the inherent defect of HAM as a film-like biomaterial. In the treatment of spinal cord defects, HAM does have a good restorative effect because of its rich extracellular matrix and a variety of nutritional molecules. However, it is difficult for the newly born neurons to reach the contralateral side through the original HAM. Acellular treatment or chemical modification did not change the structure of HAM. Only by turning HAM into a three-dimensional ordered structure can the performance of biomaterials be maximized. Fig. 3C shows the 3D structure electron micrographs of GelMA. The pore size distribution was relatively uniform and the structure was stable, with an average pore size of about 53 ± 10 μm (Fig. 3E). As shown in Fig. 3D, the structure of GelMA-HAAMMA is similar to that of GelMA. However, the pores of GelMA-HAAMMA are more uniform, and most of them are elliptical, with an average pore size of about 26 ± 9 μm (Fig. 3F). There is a very significant difference in pore size between GelMA and GelMA-HAAMMA ($p<0.05$). Considering the characteristics of newborn cells and peripheral blood-derived cells in the spinal cord defect, GelMA-HAAMMA is more suitable for guiding the recovery and regeneration of spinal cord injury.

Fig. 4A shows the maximum load values of the four groups of materials after the mechanical tensile test. The results of HAAM, HAAMMA, GelMA and

GelMA-HAAMMA were 0.47 ± 0.01 MPa, 2.51 ± 0.03 MPa, 3.35 ± 0.05 MPa and 4.18 ± 0.06 MPa, respectively. Spinal cord injury usually affects the movement of the corresponding segment of the limb. The injured site still has some degree of activity during the recovery period. In order to achieve continuous and stable degradation of composite scaffolds in the spinal cord after injury, it is necessary to have excellent elastic modulus as a support [17]. The elastic modulus of HAAM, HAAMMA, GelMA and GelMA-HAAMMA were 1.78 ± 0.07 MPa, 6.16 ± 0.12 MPa, 14.29 ± 0.24 MPa and 19.69 ± 0.52 MPa, respectively (Fig. 4B). GelMA-HAAMMA has the best elastic modulus ($p<0.05$), which ensures that it does not deform with body movement in the damaged area. In this way, the area through which the newly formed axons pass in the scaffold can be stabilized for a long time after injury [31]. The statistical results showed that the mechanical properties of the GelMA-HAAMMA group were significantly stronger than those of the other groups ($p<0.05$). The composite inherits the mechanical properties of GelMA and is superior to the pure hydrogel.

Fig. 4C represents the degradation rates of the four groups of materials. The degradation rate of HAAM is the fastest, and it is nearly completely degraded on day 10. HAAMMA is nearly 100% degraded on day 11. There is no significant difference between the two groups ($p>0.05$). Inheriting the degradation ability of GelMA, GelMA-HAAMMA is completely degraded on day 15. There is no significant difference in degradation ability between GelMA and GelMA-HAAMMA ($p>0.05$), but both of them are better than HAAM and HAAMMA ($p<0.05$). Further studies by our team could concentrate on optimizing the degradation rate.

Finally, we measured the water absorption capacity of four groups of materials. On the one hand, the biomaterial can quickly absorb water and expand, which can effectively plug and stop bleeding in the spinal cord injury area. On the other hand, biomaterials absorb nutrients from the body by absorbing water and provide a good microenvironment for cell proliferation and nerve regeneration. The swelling rate reflects the aiding effect of the biomaterial on the rapid healing of the injury. Fig. 4D summarizes the swelling rates of the four groups of materials. Unfortunately, HAM

and HAAMMA have poor absorptive capacity. They are hard to compare with the other two groups of materials on the same Y axis. We counted HAM and HAAMMA again separately (Fig. 4E). As shown in the figure, the swelling rate of GelMA-HAAMMA reached its highest peak of 407% ± 3% (n = 5) on day 24, and the swelling rate of GelMA reached its highest peak of about 497% ± 5% (n = 5) on day 28. The swelling rate of HAAM and HAAMMA reached the peak at 24 days, which was about 6.96% ± 0.14% (n = 5). The reason for the inferior results of GelMA-HAAMMA compared to GelMA group is the deficiency of absorption capacity of HAM itself [17, 28].

In vitro cell experiments

In the cellular experiment, the first thing we need to determine is whether the composite hydrogel supports neuronal growth, which is crucial for its application in SCI. The difficulty of extracting neurons is that the culture medium must be changed at the precise time point after the cells are seeded in the culture flask and the cells must be centrifuged quickly. The differential adherent separation technique was used to distinguish neurons from other cells. Therefore, it is particularly important to verify the proportion of neurons in the extracted cells. Fig. 5A shows the growth of extracted neurons in conditioned medium. Fig. 5B represents the distribution of neuronal growth under GelMA-HAAMMA co-culture conditions. Nuclei located by DAPI staining are shown in blue, and expression of neuron-specific antibodies is shown in green. Localization of nuclei in Merge images coincided with neuronal antibody staining. The results of immunofluorescence confirmed that the extracted cells were clearly neurons. By fluorescence microscopy, the characteristic morphology of neurons in the two groups of different culture environments could be clearly observed, including cell bodies, dendrites and axons. More than 90% of the cells in both groups were neurons as calculated by ImageJ software (n = 10) (Fig. 5E). According to the instructions of the cell viability staining reagent, trypan blue staining is the most convenient and convenient for statistics when the purification rate of cells is more

than 90%. Therefore, we chose the more convenient method of trypan blue staining to calculate cell survival.

At the site of SCI, neurons take up less than the total amount of nutrients that would be available under normal body conditions. GelMA-HAAMMA can continuously provide various trophic factors for nerve regeneration after application at the injury site. After verifying the proportion of neurons, we added a low concentration of medium (50% w/v) to the Control and GelMA-HAAMMA groups 1 day later to simulate the nutritional environment of the body after injury. Fig. 5C shows trypan blue cell survival images at 1d and 3d of the control group. Fig. 5D shows the results of the GelMA-HAAMMA group. Green cells in the image represent survival by color flipping of the counter. On the third day, the survival rate of the neurons in the GelMA-HAAMMA group was notably greater than that in the Control group. After 3 days, the number of surviving neurons in the GelMA-HAAMMA group was not statistically different from that before ($p>0.05$, $n = 5$). At the same time, the survival of neurons in the Control group was significantly reduced by 7% (± 1.1%) ($p<0.05$, $n = 5$). Cell survival analysis revealed that the GelMA-HAAMMA scaffold could maintain neuronal activity and had good biocompatibility with neurons. The HAAM active components in the composite hydrogel provide nutrients for neuronal growth.

In the process of SCI recovery, the rapid reconstruction of new blood vessels at the defect is also of great significance. Neovascularization is involved in nutrient transport, immune regulation and scar formation [36, 40]. Firstly, the effect of the composite hydrogel on the proliferation of HUVECs was tested. Fig. 6A shows the microscopic images of scratch experiments of cells in different groups. Fig. 6B is a quantization plot of the healing area/initial area calculated by the software. The GelMA-HAAMMA group had a mean value 0.4237 ± 0.078 higher than the Control group. The GelMA-HAAMMA group had a mean value 0.2339 ± 0.09 higher than the GelMA group ($n = 6$). The results of the cell migration assay revealed that the ability of the GelMA-HAAMMA group to promote the proliferation of HUVECs was significantly greater than that of the other groups. To further investigate the

proangiogenic ability of the composite hydrogel, Fig. 6C shows the microscopic results of the in vitro angiogenesis assay. It can be seen that the GelMA-HAAMMA group produced more neovascularization than the other two groups. In the statistical quantification plot of the number of new blood vessels (Fig. 6D), the GelMA-HAAMMA group had 111 ± 10.59 more than the Control group. The GelMA-HAAMMA group had 57.89 ± 9.307 more than the GelMA group (n = 6) [10, 29]. The composite hydrogel effectively inherits the pro-angiogenic biological activity of HAAM, which is of great help for the reconstruction of neovascularization after SCI.

Recovery from spinal cord injury in vivo

Inhibiting collagen scar formation and maintaining the stability of new tissue.

After SCI, the formation of glial scar at the injury site will become an obstacle to nerve regeneration and repair. With the extension of time, scar contracture will lead to further expansion of the defect site and even syringomyelia. Previous studies have shown that the three-dimensional structure of hydrogels can alleviate this problem without causing severe spinal cord defects. However, this can only inhibit the expansion of the injury rather than promote nerve repair [30, 31]. We first used H&E staining to observe the tissue homeostasis (Fig. 7). The results of H&E staining are usually used to observe the overall tissue morphology and local recovery. Because statistical significance is usually modest, the results shown in the figures are only for tissue homeostasis assessments. The GelMA-HAAMMA group had the least scar production and the most solid tissue recovery compared to the other groups. After overall evaluation, Masson staining was used to quantify the area of collagen scar to verify the efficacy of the composite hydrogel. As shown in Fig. 8A, the GelMA-HAAMMA group had significantly fewer areas of collagen staining than the other groups (Scale bar: 200 μm). The statistics in Fig. 8B showed that the proportion

of blue areas in the SCI group was 35.37% ± 0.7% higher than that in the Sham group. The proportion of blue area in GelMA group was 9.63% ± 0.7% higher than that in Sham group. The proportion of blue areas was 2.5% ± 0.65% higher in the GelMA-HAAMMA group (abbreviated as G-A in the figure) than in the Sham group (n = 3). The above results showed that GelMA-HAAMMA had excellent anti-glial scar formation ability as a composite hydrogel.

Improvement in motor function after spinal cord injury

The result of nerve regeneration after SCI is the gradual recovery of the body's motor function. The BBB score is recognized as a reliable index for evaluating the recovery of motor function after SCI in SD rats. As shown in Fig. 9D, the left hind limb of each SD rat showed normal motor function before surgery (score = 21). After a defect in the left spinal cord, the rats developed complete paralysis of the left hind limb. The scores of the SCI group and the GelMA group did not reach 7 at 2 weeks after the operation, which showed that the self-repair ability of the rats after SCI was limited. In the GelMA-HAAMMA group, we observed that the recovery of motor function in the SD group was clearly greater than that in the other groups at two weeks after surgery. At 4 weeks after surgery, the GelMA-HAAMMA rats were able to perform sustained palm-bearing movements and coordinated hindlimb movements with a score of 15-16. These results provide valid evidence that GelMA-HAAMMA promotes motor function recovery [32, 33].

Regeneration of neurons and axons

To further investigate the effects of GelMA-HAAMMA (abbreviated as G-A in the figure) on nerve regeneration, we performed immunofluorescence staining on the spinal cord sections of the rats at 4 weeks after surgery. We followed the same observation method for immunofluorescence as we did for section staining. We first observed the whole tissue under the microscope, and then magnified the injury site for statistics. Fig. 10 shows the overall morphology of the sectioned tissues in different groups under immunofluorescence. The blue area is the nucleus after DAPI staining. Green fluorescence is a marker of high expression of neuronal antibodies. In red,

astrocytes are labeled with GFAP antibodies. By DAPI staining, we found that the SCI group had a large number of hypertrophic scar tissue compared with other groups. The histological morphology of GelMA and GelMA-HAAMMA groups was similar to the results of Masson staining. Next, we analyzed the recovery of the injured area. As shown in Fig. 10, a large number of Tuj-1-positive neurons were detected in the G-A group, while the percentage of Tuj-1-positive neurons was lower in the SCI and GelMA groups.

Fig. 9A shows the schematic design of the animal experiment and the actual filming during the operation. According to the statistical analysis of the data (Fig. 9B), the neuronal fluorescence intensity in the SCI group was 107.4 ± 1.07 less than that in the Sham group. The fluorescence intensity of neurons in GelMA group was 82.04 ± 1.074 less than that in Sham group. The fluorescence intensity of neurons in G-A group was 38.15 ± 1.0 less than that in Sham group. Compared with other groups, the effect of G-A group on promoting nerve regeneration was very obvious, and the difference between the number of neurons in the normal spinal cord was minimal. According to the above results, GelMA-HAAMMA effectively promoted the regeneration of neurons [12, 34]. Moreover, it is worth noting that the abundance of collagen in HAAM also greatly increased the percentage of GFAP-positive cells (Fig. 9C). The fluorescence intensity of GFAP in G-A group was even higher than that in Sham group by 58.10 ± 0.58. Whether there was any other correlation between this phenomenon and HAAM remains to be further explored.

Discussion

Despite its excellent tissue regeneration potential, HAAM is limited by its thin physical shape and poor mechanical properties. It is difficult to avoid folding or tearing when dealing with thin sheets of HAAM [35]. Previous studies have shown that composite biomaterials can compensate for the defects of biomaterials by combining the active factors of biomaterials with the good mechanical properties of

scaffolds [36]. In this study, we synthesized HAAM and GelMA hydrogels as novel photocrosslinked materials with a double-layer network crossover structure. The composite had the physical and chemical properties of gelatin and inherited the biological activity of HAAM itself. In SCI, composites can effectively mimic the ECM microenvironment, regulate pathological processes, and promote neuronal regeneration. The comprehensive ability of composite materials comes from its physical properties and biological components.

GelMA is rich in hydrophilic polymers and forms a porous composite structure that can absorb large amounts of water in tissues, thus providing a good nutritional environment for cell growth and development [37]. HAAM is rich in collagen, in which the amino group reacts with MA and the methacryloyl group is transferred to form HAAMMA. The results of FTIR spectroscopy also showed that such chemical grafting was successful. The backbone structure of HAAM was not destroyed. Only when the main structure of HAAM is preserved can its biological activity be fully displayed in the recovery of SCI. Successful chemical grafting is the key to photocrosslinking of composite hydrogels.

Referring to Zhang's method [17, 19], our team used lithium phenyl phosphinate as a photoinitiator, which can complete the photocrosslinking process in a short time, to avoid long-term UV damage to DNA and cell function. After photocrosslinking, the composite scaffolds exhibited a bilayer interpenetrating structure, and the mechanical properties of HAAM were significantly enhanced.

Tissue engineering scaffolds for SCI must have sufficient biomechanical properties to support the passage of nerve axons. Excellent mechanical strength is an important prerequisite for composite hydrogels to firmly fill spinal cord defects and provide an ECM environment [38]. With the stable degradation of the composite scaffold, the newborn neurons could stably survive in the injured area. Through previous experiments, we found that the mechanical properties of GelMA-HAAMMA formed after photocrosslinking were obviously greater than those of HAAM and GelMA. The degree of chemical cross-linking of GelMA-HAAMMA is greater than that of GelMA, so water absorption is reduced, preventing significant swelling in the

spinal cord defect. SCI is often accompanied by massive bleeding. If the expansion rate of implanted biomaterials increases significantly after absorbing water, the damaged area will be severely expanded. The recovery time of the broken end of the central nervous system will be greatly extended due to the expansion of the damaged area. The swelling rate of the composite was further decreased compared with that of GelMA, proving that it does not affect the damaged area after implantation in vivo. At the same time, the deformation degree of the composite scaffold was better than those of the ordinary GelMA scaffold. As mentioned above, the composite scaffold does not change its shape during the recovery period of SCI and does not damage the regenerated nerve. Therefore, as an implantable biocomposite material, it has broad application prospects in the field of spinal cord injury.

In addition to its good mechanical properties, the scaffold retained the basement layer in the human amniotic membrane. Previous studies have shown that the mechanical properties and tensile strength of the human amniotic membrane are guaranteed by the basement membrane layer. As the extracellular matrix on which human amniotic epithelial cells (hAECs) adhere, the basement membrane contains hyaluronic acid and a variety of basal proteins, such as collagen type I, II, III, and IV, laminin-1, laminin-5, and fibronectin, which ensure the differentiation, proliferation, and migration of hAECs. Hyaluronic acid and a variety of basal proteins have excellent abilities to support nerve repair after SCI, and in the study of Hongsheng Liang et al., they demonstrated the role of the matrix in promoting axon regeneration and repairing SCI [12], which is the same as our conclusion. We suggest that GelMA-HAAMMA can strengthen the growth of newborn neurons after injury [39].

After the occurrence of SCI, the factors affecting healing are often dominated by fibrous scars and glial scars. Extensive fibrous scar production usually results in wound deformation, tearing, and void formation. Thus, it affects tissue healing. Glial scars, which are dominated by astrocytes, affect the passage of new nerve axons, leading to difficulties in nerve regeneration. The results of in vivo animal experiments showed that the tissue healing and nerve regeneration abilities of the GelMA-HAAMMA group were better than those of the other groups, which

confirmed our findings. An interesting phenomenon occurred in the GelMA-HAAMMA group, which showed that when neurons were regenerated, a large number of astrocytes were also generated. We hypothesized that abundant collagen and biological factors may promote the generation of astrocytes at the early stage of HAAM attachment to the spinal cord [33, 40]. The bilayer crossing structure of the composite scaffold may avoid the effect of astrocytes on neuronal regeneration. This phenomenon needs to be further studied. It should be noted that the degradation rate of GelMA-HAAMMA was not significantly improved compared with that of GelMA. In order to play a further role in the recovery of SCI, HAAM needs to be further modified in subsequent studies.

Currently, perfect materials do not exist in SCI related tissue engineering research. The materials designed by the researchers are made from different raw materials and have a wide range of ingredients. However, the ultimate goal of all composites is to promote central nerve regeneration. In an ideal scaffold, the newly formed axons can overcome various obstacles to pass through the injured area of SCI, resulting in the recovery of sensory and motor functions. After ensuring such an effect, we can proceed with further optimization of the composite. The GelMA-HAAMMA composite scaffold discussed in this paper is a successful first step. In the following research, we will search for bioengineering materials with better scar treatment effect and longer degradation time under the condition of ensuring the therapeutic effect, so as to promote the research of SCI recovery.

Conclusion

In this study, HAAM and MA were chemically grafted to form HAAMMA, which was subsequently photocrosslinked with GelMA gel to prepare the GelMA-HAAMMA composite scaffold. During co-culture with neurons, there was no change in cell survival after 3 days of co-culture with GelMA-HAAMMA. In the HUVECs cell proliferation assay, the healing effect of GelMA-HAAMMA group was

the most obvious. In vitro angiogenesis assay, the number of new blood vessels in GelMA-HAAMMA group was the highest. Our study confirmed that composite scaffolds can be prepared quickly and that their biological activity is not destroyed. GelMA-HAAMMA not only possesses the excellent mechanical properties of GelMA but also retains the good biocompatibility and low immunogenicity of HAAM. It is a bioactive material for tissue engineering. In the animal experiment, the spinal cord homeostasis of SD rats treated with GelMA-HAAMMA was the best. They also had the highest number of new neurons than any other group (except for Sham). In the assessment of motor function recovery, rats in the GelMA-HAAMMA group also achieved the highest BBB scores. Composite scaffolds can effectively construct the extracellular environment in spinal cord injury, regulate pathological changes and promote the generation of new neurons. The rats treated with the composites showed significant recovery of motor function after the operation. We conclude that GelMA-HAAMMA is a promising biocomposite material for central nerve repair after SCI.

Declarations

Conflicts of Competing Interest

The authors declare no competing financial interest.

Ethical Approval

All experimental procedures used in this study were approved by the Animal Care and Use Committee of Nantong University (Nantong, China) (220203322/220214810) and compliance with the National Research Council's Guide for the Care and Use of Laboratory Animals.

Consent for publication

All authors approved the publication of the article.

Author's Contributions

TX was responsible for the design of the experimental procedure, verified the composite material, participated in the whole process of experiments and wrote the

article, and was the main contributor. CWY, together with YL, was responsible for the preparation and validation of acellular amniotic membrane and the design of in vitro animal experiments. HW was responsible for photographing the in vitro cell experiments. CC was responsible for data collection for the in vitro experiments. YCZ was responsible for all data integration and collating. XQC was responsible for reviewing the correctness of the experimental design, the rigor of the experimental verification, and the final review of the paper.

Availability of Data and Material.

Data will be made available on request.Tao Xu is responsible for receiving contact to provide relevant data.

Funding

This work was supported by the National Natural Science Foundation of China (82371383).

Acknowledgment

All the authors appreciate the efforts of the Department of Obstetrics, Affiliated Hospital of Nantong University for donating human amniotic membrane and human umbilical vein endothelial cells.

Fig. 1	Schematic preparation of GelMA-HAAMMA scaffolds for spinal cord injury repair.
Fig. 2	Preparation of HAAM and HAAMMA. **(A)**Decellularization of HAM. **(B)**Results of HE staining of human amniotic membrane after decellularization. Scale bar: 100 μm (10 X). **(C)**SEM scans of HAAM and HAAMMA.Scale bar: 4 μm (10,000 X). **(D)**The difference in IR spectra between HAAM and HAMMA indicates the presence of grafting and the formation of new bonds.

Fig. 3	SEM images and pore size frequency distribution. SEM images of HAAM, HAAMMA, GelMA, and GelMA-HAAMMA are shown in panels A, B, C, and D, respectively. Scale bar: 20 μm. Plots of diameter frequency distribution data for GelMA and GelMA-HAAMMA are shown in E and F, respectively.
Fig. 4	Characterization of composite hydrogels. **(A)** Maximum load values for HAAM, HAAMMA, GelMA,and GelMA-HAAMMA.**(B)**Elastic modulus of HAAM, HAAMMA, GelMA, and GelMA-HAAMMA. **(C)** degradation rates of HAAM, HAAMMA, GelMA, and GelMA-HAAMMA. **(D)** Swelling rates of HAAM, HAAMMA, GelMA, and GelMA-HAAMMA. **(E)** Expansion rates of HAAM and HAAMMA. Data were shown as the mean ± SD (n = 5). *P＜0.05; **P＜0.01; ***P＜0.001; ****P＜0.0001; ns = not significant.
Fig. 5	Coculture of neurons and GelMA-HAAMMA. **(A)** Normal neurons. Scale bar: 200 μm (10 X). **(B)** neurons cocultured with GelMA-HAAMMA. Scale bar: 200 μm (10 X). **(C)** Survival of normal neurons after 3 days. Scale bar:5 μm (100 X). **(D)** Survival of cocultured neurons after 3 days. Scale bar:5 μm (100 X). **(E)** Statistics of neuronal purification rates. **(F)** Statistics of neuronal 3-day survival experiments.
Fig. 6	The effect of GelMA-HAAMMA on HUVECs was evaluated in vitro. **(A)** Cell migration results at 24 h. Scale bar:200 μm (5X). **(B)** Data statistics of cell migration (n = 6). **(C)** Results of tube formation after 6 h. Scale bar:200 μm (5X). **(D)** Statistics of tube formation data. Data were shown as the mean ± SD (n = 3). *P＜0.05; **P＜0.01; ***P＜0.001; ****P＜0.0001; ns = not significant.
Fig. 7	Histological analysis of the three groups 4 weeks after operation. Representative image of H&E staining. Scale bar: 200 μm (10×).
Fig. 8	Inhibition of scarring in spinal cord tissue by GelMA-HAAMMA at 4 weeks after surgery. **(A)** In representative images of Masson's trichrome staining, collagen tissue is stained blue. Scale bar: 200 μm (10×).**(B)**Data statistics of blue areas stained with collagen.
Fig. 9	Effects of GelMA-HAAMMA on neuronal growth as well as recovery of motor function. **(A)** Schematic diagram of the rat left spinal cord hemisection injury model. **(B)** Graph of the Tuj-1 IF intensity quantification. **(C)**Graph of the GFAP IF intensity quantification. **(D)** Left hind limb locomotor recovery was measured by the BBB scale. Rats treated with GelMA-HAAMMA had improved BBB locomotor scores. All data were statistically analyzed by two-way ANOVA (n = 5).Data were shown as the mean ± SD (n = 3). *P＜0.05; **P＜0.01; ***P＜0.001; ****P＜0.0001; ns = not significant.

Fig. 10	The overall image: Overall immunofluorescence images of treatment effects after spinal cord injury in the three groups. Scale bar:500 μm (4×). Locally enlarged images: Promoting effect of GelMA-HAAMMA on nerve regeneration after spinal cord injury. Tuj-1 (green) neurons, GFAP (red) astrocytes, and nuclei stained with DAPI (blue).Scale bar:100 μm (10×)

Fig. 1

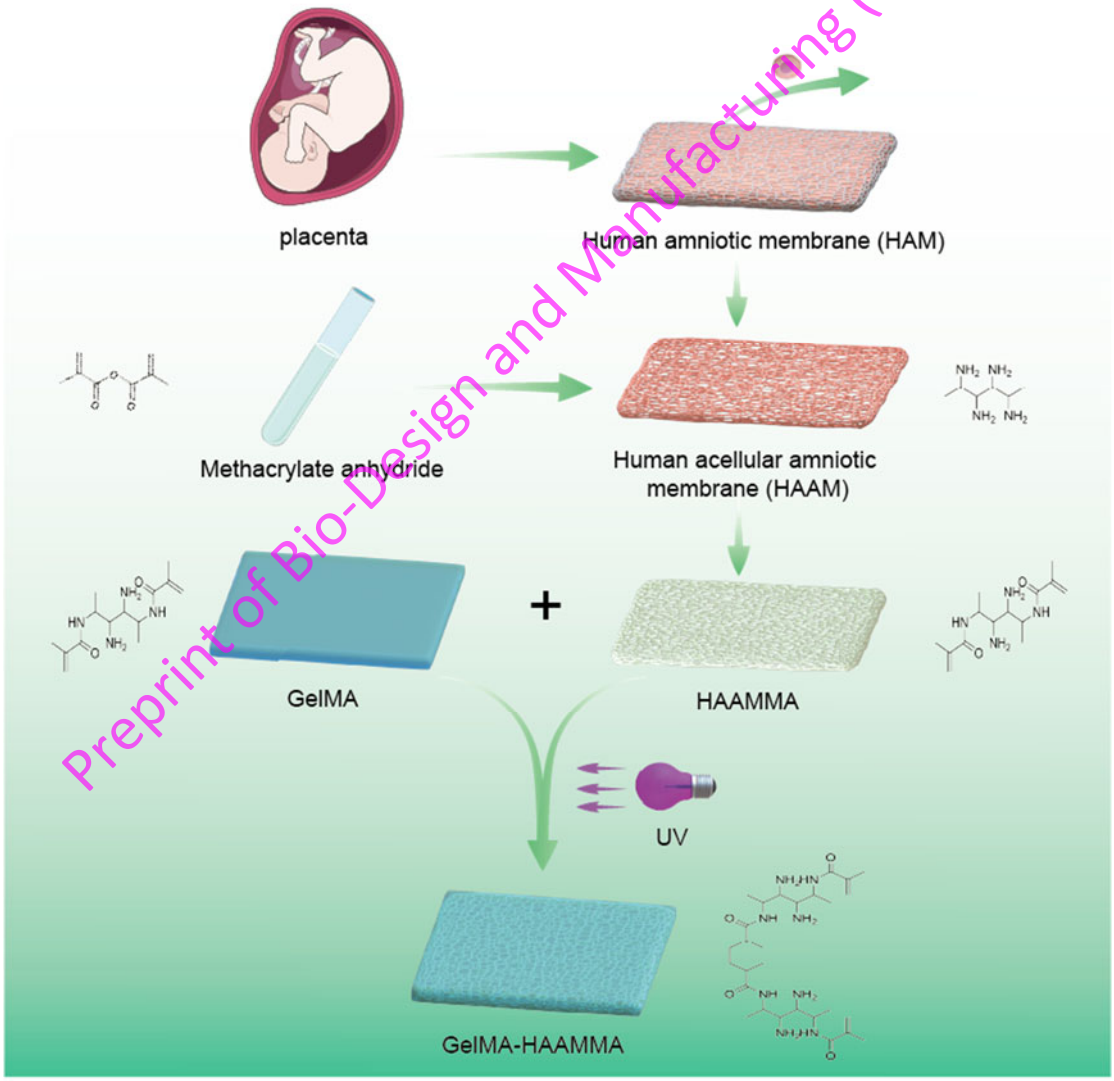

Fig. 2

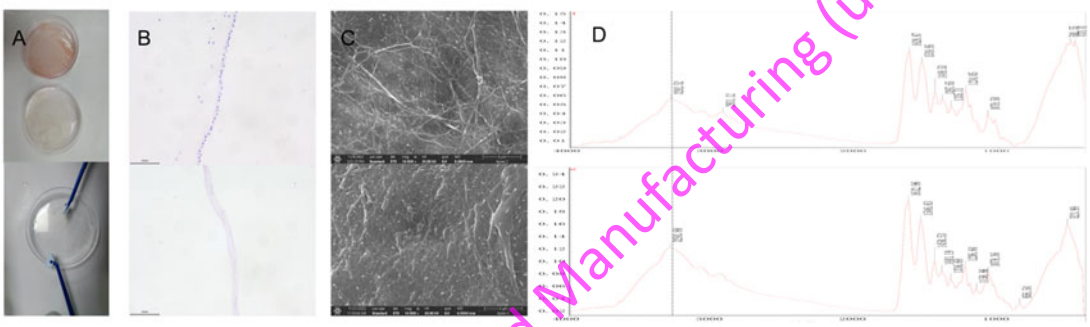

Fig. 3

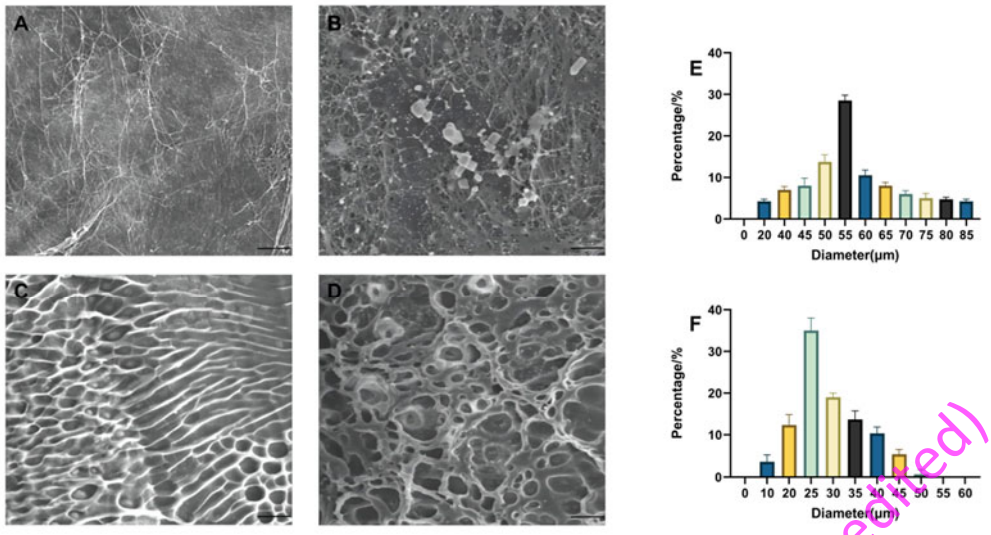

Fig. 4

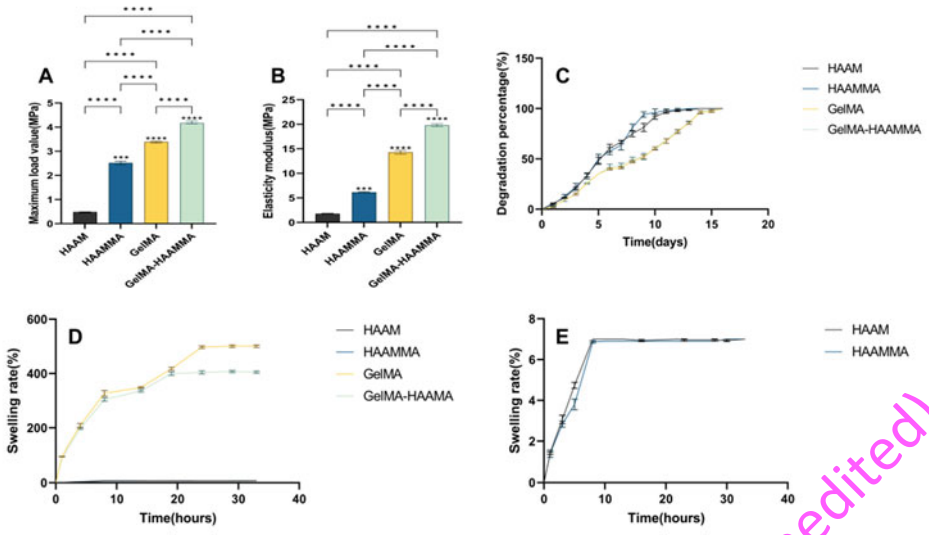

Fig. 5

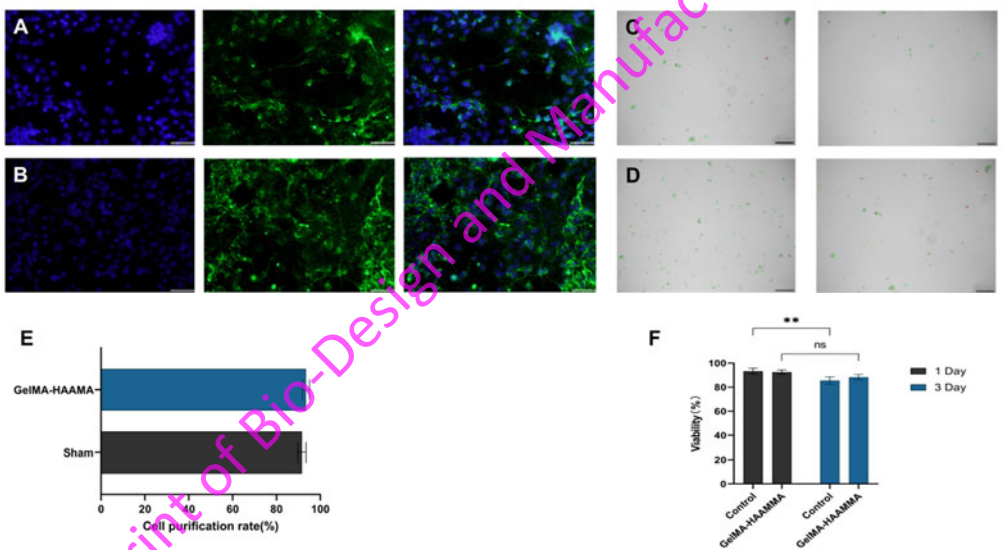

Fig. 6

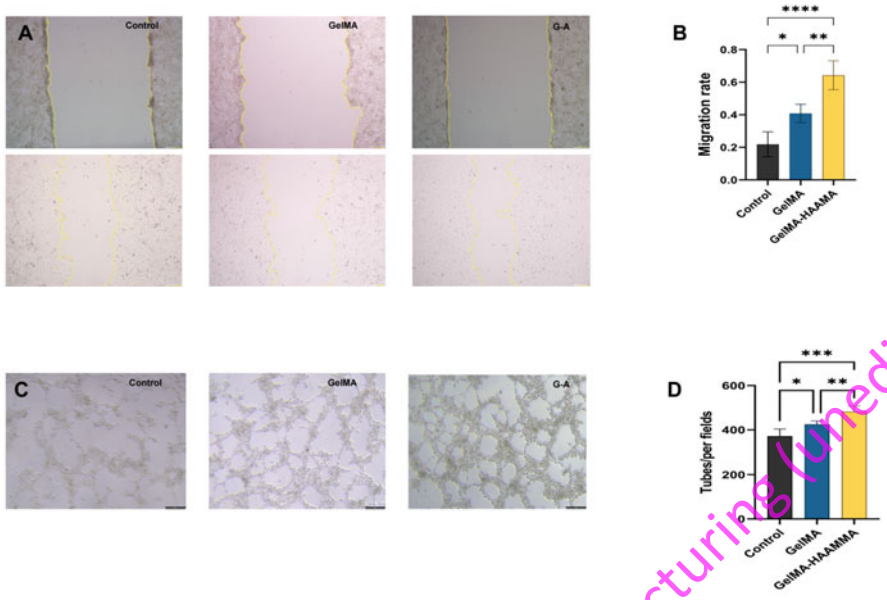

Fig. 7

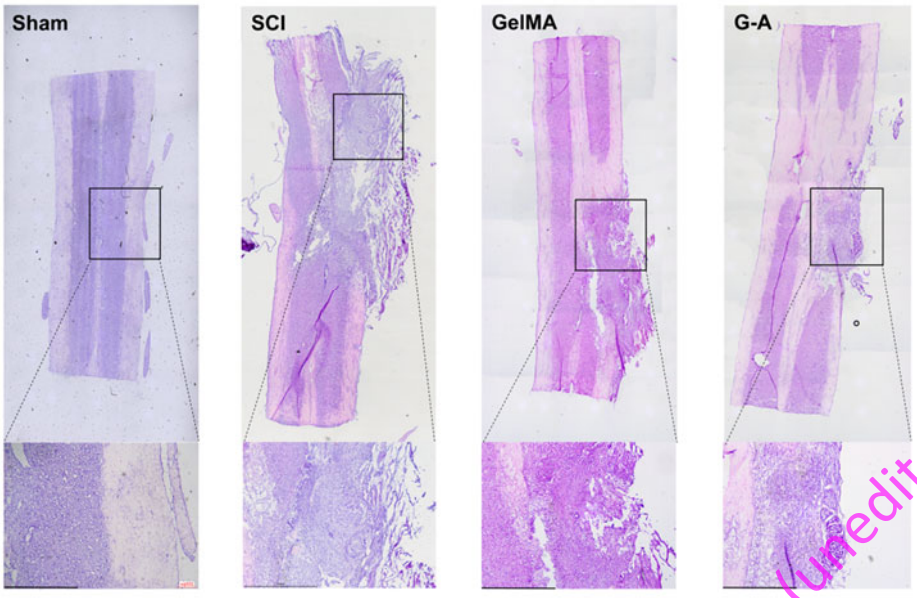

Fig. 8

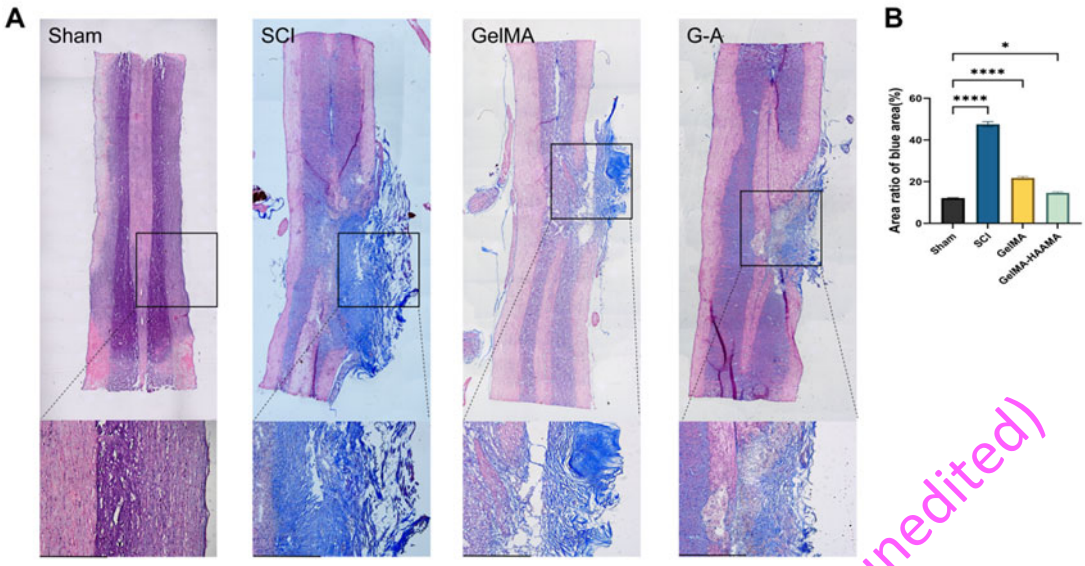

Fig. 9

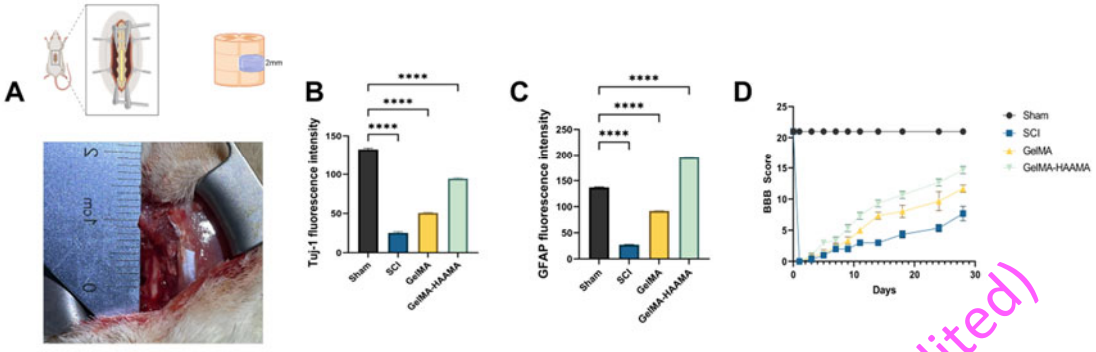

Fig. 10

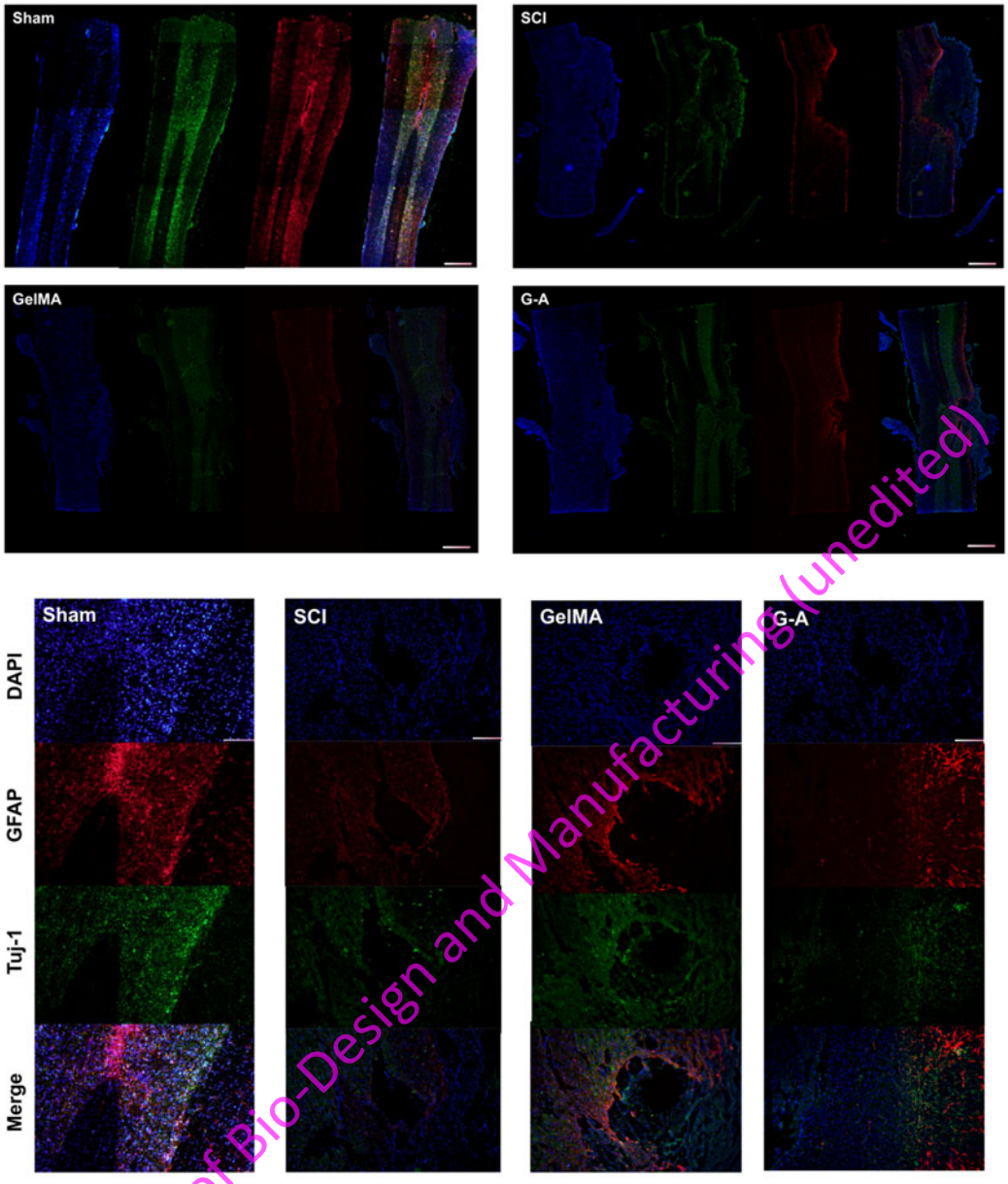

References:

[1]. Paolin, A., et al., Cytokine expression and ultrastructural alterations in fresh-frozen, freeze-dried and gamma-irradiated human amniotic membranes. Cell Tissue Bank, 2016. 17(3): p. 399-406. https://doi.org/10.1007/s10561-016-9553-x

[2]. Wang, M., et al., Application of Acellular Tissue Matrix for Enhancement of Weak Abdominal Wall in Animal Model. BioMed Research International, 2020. Mar 11: p. 1-10. https://doi.org/10.1155/2020/3475289

[3]. Wilshaw, S., et al., Biocompatibility and Potential of Acellular Human Amniotic Membrane to Support the Attachment and Proliferation of Allogeneic Cells. Tissue engineering. Part A, 2008. 14(4): p. 463-472. https://doi.org/10.1089/tea.2007.0145

[4]. Abazari, M.F., et al., Decellularized amniotic membrane Scaffolds improve differentiation of iPSCs to functional hepatocyte-like cells. J Cell Biochem, 2020. 121(2): p. 1169-1181. https://doi.org/10.1002/jcb.29351

[5]. Murphy, S.V., et al., Solubilized Amnion Membrane Hyaluronic Acid Hydrogel Accelerates Full-Thickness Wound Healing. Stem Cells Transl Med, 2017. 6(11): p. 2020-2032. https://doi.org/10.1002/sctm.17-0053

[6]. Nouri, M., et al., Healing Effects of Dried and Acellular Human Amniotic Membrane and Mepitelas for Coverage of Skin Graft Donor Areas; A Randomized Clinical Trial. Bull Emerg Trauma, 2018. 6(3): p. 195-200. https://doi.org/10.29252/beat-060302

[7]. Higa, K., et al., Hyaluronic acid-CD44 interaction mediates the adhesion of lymphocytes by amniotic membrane stroma. Cornea, 2005. 24(2): p. 206-12. https://doi.org/10.1097/01.ico.0000133999.45262.83

[8]. Gholipourmalekabadi, M., et al., Decellularized human amniotic membrane: more is needed for an efficient dressing for protection of burns against antibiotic-resistant bacteria isolated from burn patients. Burns, 2015. 41(7): p. 1488-97. https://doi.org/10.1016/j.burns.2015.04.015

[9]. Salah, R.A., I.K. Mohamed and N. El-Badri, Development of decellularized amniotic membrane as a bioscaffold for bone marrow-derived mesenchymal stem cells: ultrastructural study. J Mol Histol, 2018. 49(3): p. 289-301. https://doi.org/10.1007/s10735-018-9768-1

[10]. Xiao, S., et al., Human acellular amniotic membrane incorporating exosomes from adipose-derived mesenchymal stem cells promotes diabetic wound healing. Stem Cell Res Ther, 2021. 12(1): p. 255. https://doi.org/10.1186/s13287-021-02333-6

[11]. Mligiliche, N., et al., Extracellular matrix of human amnion manufactured into tubes as conduits for peripheral nerve regeneration. J Biomed Mater Res, 2002. 63(5): p. 591-600. https://doi.org/10.1002/jbm.10349

[12]. Liang, H., et al., DHAM-BMSC matrix promotes axonal regeneration and functional recovery after spinal cord injury in adult rats. J Neurotrauma, 2009. 26(10): p. 1745-57. https://doi.org/10.1089/neu.2008.0850

[13]. Kim, W., et al., Efficient myotube formation in 3D bioprinted tissue construct by biochemical and topographical cues. Biomaterials, 2020. Feb:230: p. 119632. https://doi.org/10.1016/j.biomaterials.2019.119632

[14]. Lei, X., et al., Research on alginate-polyacrylamide enhanced amnion hydrogel, a potential vascular substitute material. Mater Sci Eng C Mater Biol Appl, 2020.Oct: 115: p. 111145. https://doi.org/10.1016/j.msec.2020.111145

[15]. Annabi, N., et al., Engineered cell-laden human protein-based elastomer. Biomaterials, 2013. 34(22): p. 5496-505. https://doi.org/10.1016/j.biomaterials.2013.03.076
[16]. Annabi, N., et al., Engineering a sprayable and elastic hydrogel adhesive with antimicrobial properties for wound healing. Biomaterials, 2017. Sep:139: p. 229-243. https://doi.org/10.1016/j.biomaterials.2017.05.011
[17]. Zhang, Q., et al., Photo-crosslinkable amniotic membrane hydrogel for skin defect healing. Acta Biomater, 2021.Apr15: 125: p. 197-207. https://doi.org/10.1016/j.actbio.2021.02.043
[18]. Gholipourmalekabadi, M., et al., Silk fibroin/amniotic membrane 3D bi-layered artificial skin. Biomed Mater, 2018. 13(3): p. 035003. https://doi.org/10.1088/1748-605X/aa999b
[19]. Zhang, Q., et al., Development of a visible light, cross-linked GelMA hydrogel containing decellularized human amniotic particles as a soft tissue replacement for oral mucosa repair. RSC Adv, 2019. 9(32): p. 18344-18352. https://doi.org/10.1039/c9ra03009c
[20]. Zhao, X., et al., Photocrosslinkable Gelatin Hydrogel for Epidermal Tissue Engineering. Adv Healthc Mater, 2016. 5(1): p. 108-18. https://doi.org/10.1002/adhm.201500005
[21]. Sang, S., et al., Photo-crosslinked hydrogels for tissue engineering of corneal epithelium. Exp Eye Res, 2022.May: 218: p. 109027. https://doi.org/10.1016/j.exer.2022.109027
[22]. Ma, D.H., et al., Carbodiimide cross-linked amniotic membranes for cultivation of limbal epithelial cells. Biomaterials, 2010. 31(25): p. 6647-58. https://doi.org/10.1016/j.biomaterials.2010.05.034
[23]. Gage, F.H., et al., Human amnion membrane matrix as a substratum for axonal regeneration in the central nervous system. Exp Brain Res, 1988. 72(2): p. 371-80. https://doi.org/10.1007/BF00250258
[24]. Kshersagar, J., et al., Decellularized amnion scaffold with activated PRP: a new paradigm dressing material for burn wound healing. Cell Tissue Bank, 2018. 19(3): p. 423-436. https://doi.org/10.1007/s10561-018-9688-z
[25]. Wang, H., et al., Berberine-loaded MSC-derived sEVs encapsulated in injectable GelMA hydrogel for spinal cord injury repair. Int J Pharm, 2023. Aug25:643: p. 123283. https://doi.org/10.1016/j.ijpharm.2023.123283
[26]. Noor, N., et al., 3D Printing of Personalized Thick and Perfusable Cardiac Patches and Hearts. Adv Sci (Weinh), 2019. 6(11): p. 1900344. https://doi.org/10.1002/advs.201900344
[27]. Choudhury, D., et al., Organ-Derived Decellularized Extracellular Matrix: A Game Changer for Bioink Manufacturing? Trends Biotechnol, 2018. 36(8): p. 787-805. https://doi.org/10.1016/j.tibtech.2018.03.003
[28]. Bajpai, I., et al., Response of human bone marrow-derived MSCs on triphasic Ca-P substrate with various HA:TCP ratio. J Biomed Mater Res B Appl Biomater, 2017. 105(1): p. 72-80. https://doi.org/10.1002/jbm.b.33538
[29].Wu, Z., et al., Human acellular amniotic membrane is adopted to treat venous ulcers. Exp Ther Med, 2018. 16(2): p. 1285-1289. https://doi.org/10.3892/etm.2018.6331
[30]. Mohammad, J., et al., Modulation of peripheral nerve regeneration: a tissue-engineering approach. The role of amnion tube nerve conduit across a 1-centimeter nerve gap. Plast Reconstr Surg, 2000. 105(2): p. 660-6. https://doi.org/10.1097/00006534-200002000-00027
[31]. Bankiewicz, K.S., et al., Reversal of hemiparkinsonian syndrome in nonhuman primates by amnion implantation into caudate nucleus. J Neurosurg, 1994. 81(6): p. 869-76. https://doi.org/10.3171/jns.1994.81.6.0869
[32]. Liu, X., et al., 3D bioprinted neural tissue constructs for spinal cord injury repair. Biomaterials, 2021. May:272: p. 120771. https://doi.org/10.1016/j.biomaterials.2021.120771

[33]. Shen, H., et al., A DAMP-scavenging, IL-10-releasing hydrogel promotes neural regeneration and motor function recovery after spinal cord injury. Biomaterials, 2022.Jan: 280: p. 121279. https://doi.org/10.1016/j.biomaterials.2021.121279
[34]. Sadraie, S.H., et al., Study of Transected Sciatic Nerve Repair by Amniotic Membrane with Betamethasone in Adult Albino Wistar Rats. Arch Iran Med, 2016. 19(9): p. 612-7.
[35]. Clayman, G.L., R. Roy and J. Norman, Human Amnion/Chorion Membrane May Reduce Transient Recurrent Laryngeal Nerve Injury During Thyroid Surgery. Cell Transplant, 2022. Jan-Dec:31: p. 9636897211073136. https://doi.org/10.1177/09636897211073136
[36]. Yang, Y., et al., small molecules combined with collagen hydrogel direct neurogenesis and migration of neural stem cells after spinal cord injury. Biomaterials, 2021. Feb:269: p. 120479. https://doi.org/10.1016/j.biomaterials.2020.120479
[37].Yue, K., et al., Synthesis, properties, and biomedical applications of gelatin methacryloyl (GelMA) hydrogels. Biomaterials, 2015.Dec: 73: p. 254-71. https://doi.org/10.1016/j.biomaterials.2015.08.045
[38]. Fan, C., et al., Restoration of spinal cord biophysical microenvironment for enhancing tissue repair by injury-responsive smart hydrogel. Biomaterials, 2022. Sep:288: p. 121689. https://doi.org/10.1016/j.biomaterials.2022.121689
[39]. Mohammad, J.A., et al., Increased axonal regeneration through a biodegradable amnionic tube nerve conduit: effect of local delivery and incorporation of nerve growth factor/hyaluronic acid media. Ann Plast Surg, 2000. 44(1): p. 59-64. https://doi.org/10.1097/00000637-200044010-00010
[40]. Liu, X., et al., A functionalized collagen-I scaffold delivers microRNA 21-loaded exosomes for spinal cord injury repair. Acta Biomater, 2022.Dec: 154: p. 385-400. https://doi.org/10.1016/j.actbio.2022.10.027